Helicity, topology, and Kelvin waves in reconnecting quantum knots

P. Clark di Leoni,[1] P. D. Mininni,[1] and M. E. Brachet[2]

[1]*Departamento de Física, Facultad de Ciencias Exactas y Naturales, Universidad de Buenos Aires and IFIBA, CONICET, Ciudad Universitaria, 1428 Buenos Aires, Argentina*

[2]*Laboratoire de Physique Statistique de l'Ecole Normale Supérieure associé au CNRS et aux Universités Paris 6 et 7, 24 Rue Lhomond, 75237 Paris Cedex 05, France*

(Received 29 February 2016; revised manuscript received 22 April 2016; published 3 October 2016)

Helicity is a topological invariant that measures the linkage and knottedness of lines, tubes, and ribbons. As such, it has found myriads of applications in astrophysics, fluid dynamics, atmospheric sciences, and biology. In quantum flows, where topology-changing reconnection events are a staple, helicity appears as a key quantity to study. However, the usual definition of helicity is not well posed in quantum vortices, and its computation based on counting links and crossings of centerline vorticity can be downright impossible to apply in complex and turbulent scenarios. We present a definition of helicity which overcomes these problems and which gives the expected result in the large-scale limit. With it, we show that certain reconnection events can excite Kelvin waves and other complex motions of the centerline vorticity, which slowly deplete helicity as they interact nonlinearly, thus linking the theory of vortex knots with observations of quantum fluids. This process also results in the depletion of helicity in a fully turbulent quantum flow, in a way reminiscent of the decay of helicity in classical fluids.

DOI: 10.1103/PhysRevA.94.043605

I. INTRODUCTION

Helicity plays an important role in the dynamics of many fluid flows, from astrophysics [1] to geophysics [2–4]. It is a measure of the knottedness of field lines, which is conserved under appropriate conditions, and as such it has been called a "topological invariant" of many flows [5]. These ideas [6–9] have found applications in areas beyond fluid dynamics, such as DNA biology [10], optics [11], and electromagnetism [12]. Although helicity is perfectly conserved in barotropic ideal fluids, in real fluids [13,14], and in superfluids [15–17], vortex reconnection events, which alter the topology of the flow, can take place. It is unclear if helicity is preserved under reconnection. Experiments of vortex knots in water have shown that centerline helicity remains constant throughout reconnection events [18], while theoretical arguments indicate that writhe (one component of the helicity) should be conserved in antiparallel reconnection events [19], a fact later confirmed in numerical simulations of a few specific quantum vortex knots [20]. However, numerical studies of Burgers-type vortices indicate that helicity is not conserved [21]. While experiments studying helicity in quantum flows have not been done yet, the recent experimental creation of quantum knots in a Bose-Einstein condensate [22] is a significant step in that direction.

Recently, quantum flows have been used as a testbed for many of these ideas [18,20,23], as vorticity in a quantum flow is concentrated along lines with quantized circulation, and as these can reconnect without dissipation. However, the lack of a fluidlike definition of helicity for a quantum flow requires complex topological measurements of the linking and knottedness of the centerline vorticity [18,23], or artificial filtering of the fields [20] to prevent spurious values of helicity resulting from the singularity near quantum vortices. Moreover, reconnection events in superfluids can excite Kelvin waves [24] (helical perturbations that travel along the vortices first predicted for classical vortices [25]). These are believed to be responsible for the generation of an energy cascade [26,27] leading to Kelvin wave turbulence [28]. Possible links between helicity and the development of turbulence have remained obscure as a result of the difficulties involved in the measurement of both helicity and Kelvin waves.

Here we study the time evolution of helicity and its link with Kelvin waves in numerical simulations of the Gross-Pitaevskii equation (GPE). The GPE models superfluids and Bose-Einstein condensates (BECs) near zero temperature. We present a fluidlike regularized definition for the helicity, which solves the problem arising from the singularities in the velocity and vorticity produced by the topological defects in the quantum flow, and links quantum knots with helicity as measured in fluid dynamics. We study its time evolution in multiple linked rings and knots and show that only some reconnection events conserve helicity, while in others helicity decays towards a new constant value. We link the depletion of helicity in the latter case to the excitation of complex motions of the centerline vorticity and of a nonlinear transfer of energy in Kelvin waves, which ultimately results in the radiation of phonons. Finally, we illustrate how the regularized helicity can be successfully used to quantify the helicity in complicated and turbulent situations.

II. HELICITY IN QUANTUM FLOWS

Low temperature quantum flows and BECs can be modeled as a field of weakly interacting bosons of mass m using the GPE,

$$i\hbar\frac{\partial\Psi}{\partial t} = -\frac{\hbar^2}{2m}\nabla^2\Psi + g|\Psi|^2\Psi, \tag{1}$$

where Ψ is the system's wave function and g is proportional to the scattering length. The total energy, which is conserved by the GPE, can be decomposed into three components. First,

the so-called "classical" kinetic energy density is defined as

$$E_k = \tfrac{1}{2}\rho|\mathbf{v}|^2, \tag{2}$$

where $\rho = mn$ is the mass density, n is the particle density, and $\mathbf{v}$ is the flow velocity, all obtained in terms of the wave function (see below). Using a Helmholtz decomposition of the flow velocity, this energy can be further decomposed into a kinetic energy associated with compressible motions E_k^c, and an energy associated with incompressible motions E_k^i. Second, the so-called quantum energy is

$$E_q = \frac{\hbar^2}{2m^2}(\nabla\sqrt{\rho})^2. \tag{3}$$

Finally, the potential (or internal) energy is given by

$$E_p = \frac{g}{2m^2}\rho^2. \tag{4}$$

A detailed study of the energy decomposition in the GPE can be found in [29,30].

The flow from the GPE matches the behavior of a classical, ideal, and compressible potential fluid, except at points where a topological singularity takes place. These topological defects take place when $\Psi = 0$ and are the so-called quantum vortices whose circulation is quantized and given by $\Gamma = \oint_C \mathbf{v}(\ell)\, d\ell = 4\pi\alpha$, with $\alpha = \hbar/(2m)$. The vorticity ω of the flow is thus

$$\boldsymbol{\omega}(\mathbf{r}) = \Gamma \int ds \frac{d\mathbf{r}_0}{ds}\delta^{(3)}[\mathbf{r} - \mathbf{r}_0(s)], \tag{5}$$

where $\mathbf{r}_0(s)$ is the position of the $\Psi = 0$ centerline, and s is the arc length.

From the wave function, the particle density is given by $n = \overline{\Psi}\Psi$, and the velocity field can be obtained from

$$\mathbf{v} = \frac{\mathcal{P}}{n}, \quad \mathcal{P}_j = 2\alpha\frac{\overline{\Psi}\partial_j\Psi - \Psi\partial_j\overline{\Psi}}{2\,i}, \tag{6}$$

where $\mathcal{P}$ is the unit mass momentum density. At a distance $r \to 0$ from a straight vortex these quantities are known [29] to behave as $n \sim r^2$ and $\mathbf{v} = 2\alpha\mathbf{e}_\theta/r$, where $\mathbf{e}_\theta$ is the azimuthal unit vector and r is the radial distance in a cylindrical coordinate system $(\mathbf{e}_r, \mathbf{e}_\theta, \mathbf{e}_z)$ having its origin on the straight vortex. Thus, the velocity $\mathbf{v}$ has an r^{-1} singularity *perpendicular* to the centerline.

As the vorticity also has a singularity *perpendicular* to those lines, the standard definition of helicity

$$\mathcal{H} = \int d\mathbf{r}\, \boldsymbol{\omega}(\mathbf{r}) \cdot \mathbf{v}(\mathbf{r}) \tag{7}$$

is not well behaved, as it involves the product of two singular distributions. The idea of the *regularized* helicity is to replace in Eq. (7) the field $\mathbf{v}$ by a regularized smooth field $\mathbf{v}_{\rm reg}$ having no divergences perpendicular to the line, and the same regular behavior as $\mathbf{v}$ parallel to the line.

We can regularize the velocity along the centerline by Taylor expanding Ψ to first order in the numerator and the denominator in Eq. (6), arriving at

$$v_\parallel = \frac{2\alpha}{2i}\frac{\mathcal{W}_j\{[\partial_j\partial_l\Psi)\partial_l(\overline{\Psi})] - [\partial_j\partial_l\overline{\Psi})\partial_l(\Psi)]\}}{\sqrt{\mathcal{W}_l\mathcal{W}_l}(\partial_m\Psi)(\partial_m\overline{\Psi})}, \tag{8}$$

where $\mathcal{W}_j = \epsilon_{jkl}\partial_k\mathcal{P}_l$ is a smooth field oriented along the vortex. We define the regularized helicity as

$$\mathcal{H} = \int d\mathbf{r}\, \boldsymbol{\omega}(\mathbf{r}) \cdot \mathbf{v}_{\rm reg}(\mathbf{r}), \tag{9}$$

with $\mathbf{v}_{\rm reg} = v_\parallel \mathcal{W}/\sqrt{\mathcal{W}_j\mathcal{W}_j}$.

The definition of the regularized helicity in Eq. (9) is well behaved in the sense of standard distribution theory [31], as it is the integral of the product of a distribution ($\boldsymbol{\omega}$) with a well-behaved function ($\mathbf{v}_{\rm reg}$). As such, it can be computed numerically (e.g., in standard pseudospectral methods, in Fourier space using Parseval identity), and should converge algebraically. Although the choice of regularizing $\mathbf{v}$ (instead of $\boldsymbol{\omega}$) may seem arbitrary, it is not. The vorticity as given in Eq. (5) corresponds to an exact solution of the GPE. On the other hand, the singular behavior of the velocity in the direction *parallel* to the centerline is the result of a 0/0 indeterminate form in the expression for $\mathbf{v}$, as it follows directly from Eq. (6) because $\Psi = 0$ in the centerline. As such, the regularization of the velocity in Eq. (8) can be seen simply as l'Hôpital regularization to remove the indeterminacy when $\Psi = 0$.

Next we show how this regularized helicity still holds the geometrical interpretations valid for the standard (or classical) one.

A. Relation with writhe

For an isolated structure helicity can be decomposed into twist Tw, and writhe Wr. For a single curve we have [32]

$$\mathrm{Wr} = \frac{1}{4\pi}\frac{\int\int(d\mathbf{r}\times d\mathbf{r}_1)\cdot(\mathbf{r}-\mathbf{r}_1)}{|(\mathbf{r}-\mathbf{r}_1)|^3}. \tag{10}$$

It is easy to see that if one uses a velocity field $\mathbf{V}(\mathbf{r})$ given by the Biot-Savart law

$$\mathbf{V}(\mathbf{r}) = \frac{\Gamma}{4\pi}\frac{\int d\mathbf{r}_1\times(\mathbf{r}-\mathbf{r}_1)}{|(\mathbf{r}-\mathbf{r}_1)|^3}, \tag{11}$$

where $\mathbf{r}_1$ corresponds to the position of the centerline, and the vorticity as defined in Eq. (5), then the helicity $\mathcal{H}$ is given by

$$\mathcal{H} = \frac{\Gamma^2}{4\pi}\frac{\int\int d\mathbf{r}\cdot[d\mathbf{r}_1\times(\mathbf{r}-\mathbf{r}_1)]}{|(\mathbf{r}-\mathbf{r}_1)|^3}.$$

From the identity $(\mathbf{a}\times\mathbf{b})\cdot\mathbf{c} = \mathbf{a}\cdot(\mathbf{b}\times\mathbf{c})$ one finds that in this simple case (for a *single* line), $\mathcal{H} = \Gamma^2\mathrm{Wr}$.

B. Regularized helicity defined as the twist of constant phase ribbon

Let us recall that the twist Tw of a ribbon [defined by *both* a curve $\mathbf{r}(s)$, and a vector $\mathbf{U}(s)$ perpendicular to the curve] is defined by

$$\mathrm{Tw} = \frac{1}{2\pi}\int\left(\mathbf{U}\times\frac{d\mathbf{U}}{ds}\right)\frac{d\mathbf{r}}{ds}ds = N + \frac{1}{2\pi}\int\tau(s)ds, \tag{12}$$

where τ is the torsion, and N the number of turns around the curve of $\mathbf{U}$ in the Frenet-Serret frame (see the Appendix A). Under the GPE, constant phase surfaces will intersect on the centerline. Now consider a line at a close distance of the vortex and lying on a constant phase surface. The centerline and the

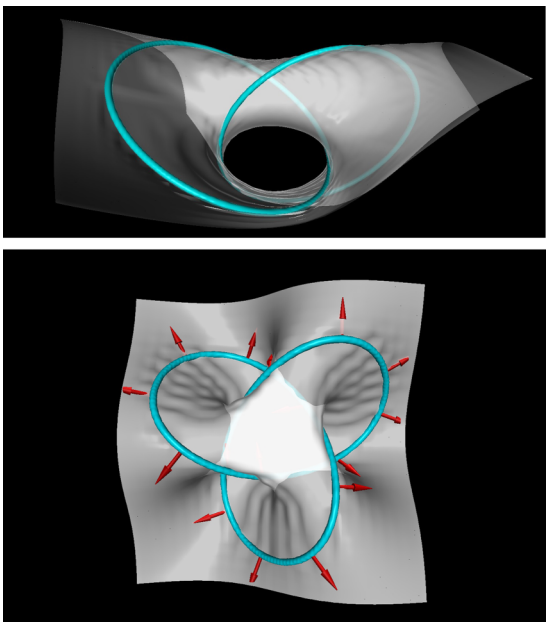

FIG. 1. Renderings of the surface of zero phase for two knots in a quantum fluid. Top: Two linked rings, note the surface has one hole. Bottom: Trefoil knot, with three holes. The number of holes is associated with the number of turns the vector that lies on the surface perpendicular to the vortex does as it moves along the curve (a few of these vectors are shown).

constant phase line define a ribbon. Using Eqs. (5) and (12) we can see that $\mathcal{H} = -\Gamma^2\,\mathrm{Tw}$.

Figure 1 shows renderings of surfaces of zero phase for two knots in a quantum fluid. A hole indicates that the vector perpendicular to the vortex lying on this surface does a whole turn as it moves along the vortex, thus making a contribution of one quantum to the intrinsic twist. The arrows in Fig. 1 show examples of the direction of this vector at different places (see also the Supplemental Material [33] for an animation of these knots).

III. METHODS

A. Numerical scheme

To study the time evolution of helicity in different configurations, the GPE equations were integrated using GHOST [34–36], a three-dimensional code which uses a pseudospectral scheme with periodic boundary conditions to compute spatial derivatives and a fourth order Runge-Kutta scheme to compute time derivatives. The "2/3 rule" is used for de-aliasing. The code is parallelized using both MPI and OpenMP. We consider two sets of simulations. The vortex knots simulations were done using 256^3 grid points (other simulations at different resolutions were performed to check numerical convergence, but only the results from the simulations with 256^3 grid points are shown below). The largest simulation of an ABC flow (a turbulent helical flow) discussed below was done with 2048^3 grid points, also with simulations performed at lower resolution to verify convergence.

B. Preparation method for vortex knots

The initial data preparation method is based on the one presented in [18]. The method consists of calculating the velocity field generated by a vortex line (or lines) $\mathbf{r}(s)$, which is then integrated to get the phase of the wave function. The density at each point in space is then calculated by using a Padé approximation. One of the two differences with the method presented in [18] is that after doing this we first use the generated wave function as an initial condition of the advected real Guinzbug Landau equation (ARGLE), whose stationary solutions are solutions of the GPE with minimal acoustic energy [29], and then feed that solution to the GPE, thereby minimizing errors (specially those stemming from the Padé approximation [17]). The other key difference is that our fields are truly periodic. Instead of using an array of replicas to generate an almost periodic field, we work in the Fourier domain using the Fourier transform of the vorticity in Eq. (5), which as we evaluate only at integer wave numbers gives a perfectly periodic field. The velocity field is then obtained by applying the inverse of the curl operator (i.e., the Biot-Savart law).

C. Preparation method for quantum ABC flow

The so-called ABC (Arnold, Beltrami, and Childress) velocity field is a maximal helicity stationary solution of Euler equations in which the vorticity is parallel to the velocity, explicitly given by

$$\begin{aligned}\mathbf{u}_{\mathrm{ABC}}(x,y,z) = \{&[B\cos(ky) + C\sin(kz)]\hat{x}\\ &+ [A\sin(kx) + C\cos(kz)]\hat{y}\\ &+ [A\cos(kx) + B\sin(ky)]\hat{z}\}. \end{aligned} \tag{13}$$

This velocity is the sum of three simple ($A = B = 0$, $A = C = 0$, and $B = C = 0$) flows. We first construct an ARGLE initial wave function for each of these flows, and then take their product and evolve the ARGLE in time to minimize errors and the acoustic energy.

In particular, it is easy to see that the $A = B = 0$ flow is a constant z-dependent advection in each x-y slice. By Madelung's transformation the constant advection $C[\sin(kz)\hat{x} + \cos(kz)\hat{y}]$ should correspond to a wave function

$$\Psi(x,y,z) = e^{i\frac{C\sin(kz)}{2\alpha}x + \frac{C\cos(kz)}{2\alpha}y}. \tag{14}$$

In order to have 2π-periodic initial data we initially set

$$\Psi(x,y,z) = e^{i[\frac{C\sin(kz)}{2\alpha}]x + [\frac{C\cos(kz)}{2\alpha}]y}, \tag{15}$$

where $[a]$ stands for the integer nearer to a.

The general initial data are made out of a product of such functions, corresponding to nonzero A, B, and C, and various values of the wave number k. Note that the frustration [the relative difference between $C\sin(kz)/(2\alpha)$ and an integer] goes down when $\alpha = c\xi/\sqrt{2} \to 0$.

IV. EVOLUTION OF QUANTUM KNOTS

A. Dynamics of helicity

We consider four different initial conditions: one unknotted ring, two unknotted but linked rings, a trefoil knot, and a (1,6)-

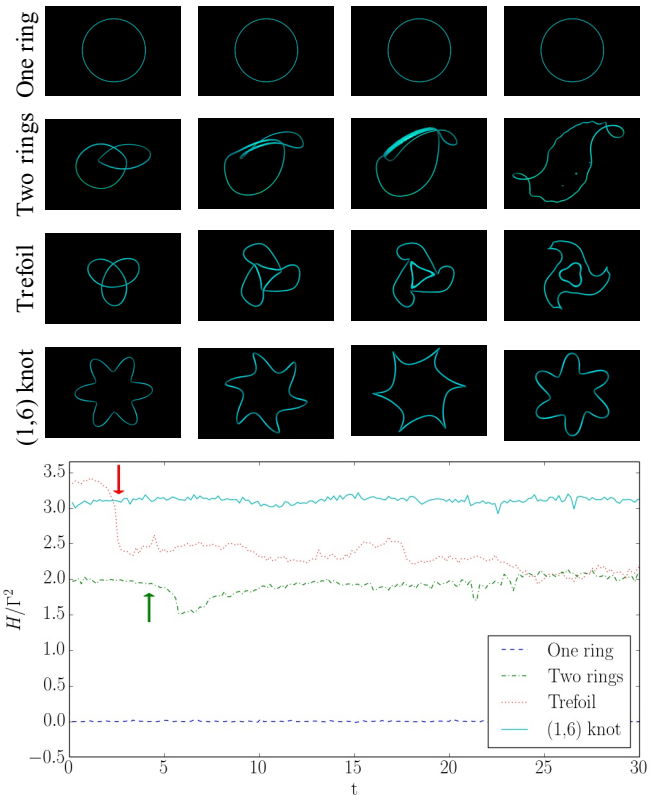

FIG. 2. Time evolution of the helicity for four quantum vortex configurations. At the top, snapshots of the configurations at different times are shown. The single ring only moves at constant speed. The two rings and the trefoil reconnect at times marked by the vertical arrows. When reconnection takes place between two perfectly antiparallel vortices (as in the two rings), helicity does not change. In the trefoil reconnection takes place simultaneously at three points and helicity changes abruptly at the time indicated by the red arrow; later it decays slowly to its final value. The (1,6)-torus knot deforms without reconnecting, and its helicity does not change.

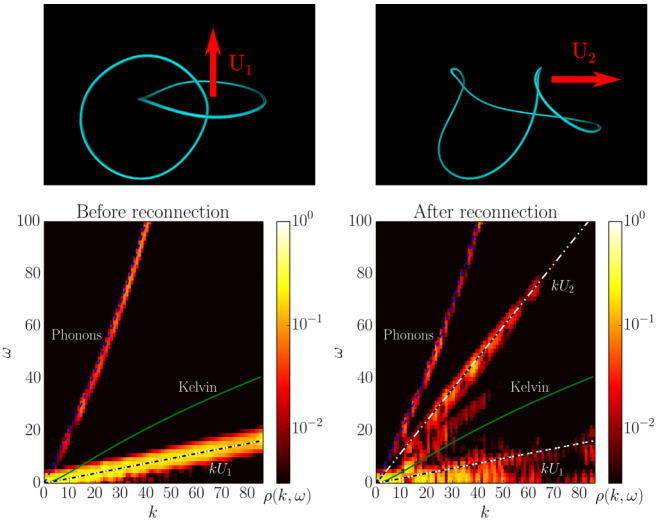

FIG. 3. Spatiotemporal spectrum for the two rings before (left) and after reconnection (right). The dashed (blue) line corresponds to the dispersion relation of sound waves, the solid (green) line to Kelvin waves, the dash-dotted line to sweeping with velocity U_1 (i.e., $\omega = U_1 k$), and the dash-triple dotted line to sweeping with $\omega = U_2 k$. Sweeping concentrates most of the power, and only one energetic mode with $k \approx 11$ may be compatible with the dispersion relation of Kelvin waves.

torus knot. Snapshots at different times during their evolution are shown in Fig. 2. The evolution of the regularized helicity (normalized by Γ^2) for each configuration as a function of time is also shown in Fig. 2. A red and a green arrow mark the moment when the trefoil and the two rings reconnect, respectively.

All four configurations start at the expected value of helicity (which we verified with other methods to compute helicity in quantum flows [20]). The single ring moves at constant velocity parallel to its axis without deformations, and helicity remains constant at zero. The two rings move towards each other, and align to reconnect two long antiparallel segments (see the third panel of the snapshots). At that time there is a small drop of the regularized helicity (associated with the fact that the regularization is not well defined while reconnection takes place), but then the helicity remains constant around its original value of 2, even though there remains only one ring after reconnection. This is to be expected for antiparallel reconnection, as predicted in [19], and in agreement with previous results [18,23]. As is clear from the visualizations, the helicity in the link of the two rings gets converted into a helical deformation (writhe) of the single ring. The trefoil reconnects at three points simultaneously, but the vortices are not perfectly antiparallel at the moment of reconnection. Centerlines always form coplanar hyperbolas [37,38] and align antiparallely, but as vortices have a finite size in the GPE, reconnection can start before vortices can perfectly align leading to the described situation [18]. As a result, helicity rapidly drops by one quantum from an initial value of ≈ 3.4. Remarkably, it then continues dropping slowly until it reaches a new steady value of 2 quanta at $t \approx 25$. As will be shown next, this decay is associated with the excitation of helical waves along the two vortex rings resulting from the reconnection. Finally the (1,6)-torus knot deforms substantially as it evolves, but its helicity remains around its initial value. Videos showing the evolution in each case can be found in the Supplemental Material [33].

To sum up, there exist stable helical solutions of the GPE where vortex knots do not reconnect, antiparallel reconnections conserve helicity in agreement with previous studies [19,20], but in disagreement with previous studies helicity is not always conserved. Even after reconnection helicity can vary slowly by a yet unclear mechanism. Below we show that this mechanism is the emission of phonons by the nonlinear interaction of helical Kelvin waves and other deformations excited along the centerline.

B. Kelvin waves excitation by reconnection

To understand the process that results in the slow depletion of helicity, we compute the spatiotemporal spectrum of mass density $\rho(k,\omega)$, before and after the reconnection, for the two rings (Fig. 3) and for the trefoil (Fig. 4). This spectrum is a useful tool to identify waves and flow displacements in

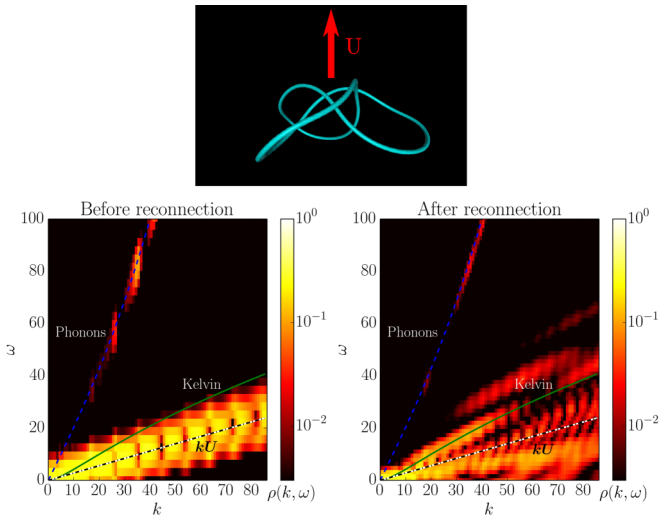

FIG. 4. Spatiotemporal spectrum for the trefoil before (left) and after the reconnection (right). The dashed (blue) line corresponds to sound waves, the solid (green) line to Kelvin waves, and the dash-dotted line to sweeping with $\omega = Uk$. A broad range of modes compatible with the dispersion relation of Kelvin waves is excited after reconnection, and sound waves are visible at high frequencies.

complex flows [28,39]. The GPE can sustain two types of waves that will be of interest in the following: sound waves which follow the Bogoliubov dispersion relation $\omega_B(k) = ck\sqrt{1+\xi^2k^2/2}$, where $c = \sqrt{g|\Psi|^2/m}$ is the speed of sound and $\xi = \sqrt{\hbar^2/(2mg|\Psi|^2)}$ is the coherence length [29], and Kelvin waves which follow $\omega_K(k) = 2c\xi/(\sqrt{2}a^2)[1 \pm \sqrt{1+K_0(ka)/K_1(ka)}]$, where a is the radius of the vortex core and K_0 and K_1 are modified Bessel functions.

In Fig. 3, before reconnection takes place, the two rings move towards each other at a mean velocity U_1. This appears in the spatiotemporal spectrum as sweeping of the vortices, i.e., a concentration of power near the region with $\omega = U_1k$ (excitations corresponding to sound waves can also be identified). After reconnection, the vortex still moves slowly with a velocity close to U_1, but the reconnected points separate fast from each other with velocity U_2, thus concentrating energy along $\omega = U_2k$. Only at $k \approx 11$ does there seem to be an almost monochromatic Kelvin wave excitation. Indeed, in the last snapshot of the two rings in Fig. 2, a small helical perturbation with this wave number can be observed (see also the video in the Supplemental Material [33]).

The spatiotemporal spectrum for the trefoil, for which helicity is not conserved, is very different. Before reconnection the vortex knot moves with mean velocity U, and sweeping with $\omega = Uk$ can be observed in the spectrum. After reconnection the motion of the two rings is complex, although both structures still move with an average velocity U. But the most remarkable feature in the spectrum is the excitation of a broad and continuous range of modes compatible with the dispersion relation of Kelvin waves, which indicates the development of nonlinear interactions of Kelvin waves. As only one vortex knot is present, the system does not develop a fully turbulent cascade (see [28] for a study of spatiotemporal spectra in the case of fully developed turbulence in GPE).

The excitation of Kelvin waves with multiple wavelengths in the trefoil creates a transfer of energy and helicity to the smaller scales where it can be dissipated by phonon emission [40], as is evidenced by the excitation of sound waves at only high frequencies in Fig. 4. Kelvin waves fade away once helicity reaches its new steady state value of $\approx 2\Gamma^2$. Note that in Figs. 3 and 4 other modes are also excited. Sweeping with $\omega = Uk$ is a particular case of a more general spectrum with $\omega \propto k^r$ predicted for a randomly stirred vortex loop [41,42]. The data is thus compatible with such deformations of the centerline.

V. HELICITY IN QUANTUM TURBULENCE

Finally, we show the regularized helicity is robust even for quantum turbulence, where hundreds of thousands of knots can be present in the flow. Figure 5 shows the three-dimensional rendering of a helical flow, with a distribution of vortices such that the flow large-scale structure corresponds to the classical ABC flow. A grid of 2048^3 points was used. Computation of the regularized helicity over the quantum flow gives the expected value of 3, matching the classical value. In units of Γ^2 this value corresponds to $\approx 480\,000$ links.

Figure 6 shows the evolution of the helicity and of the different components of the total energy, in a simulation with the same initial conditions but using 1024^3 grid points. Note that the total energy (i.e., the sum of all components) remains constant through the simulation, as expected for the GPE. As expected from previous results [28,29], the incompressible kinetic energy decays into the other energy components, mainly as the result of the emission of phonons produced by the energy cascade (note the growth of E_k^c at late times). In other words, the flow first evolves into a turbulent state dominated by incompressible motions (note E_k^i remains approximately constant as turbulence develops, up to $t \approx 4$), and afterwards

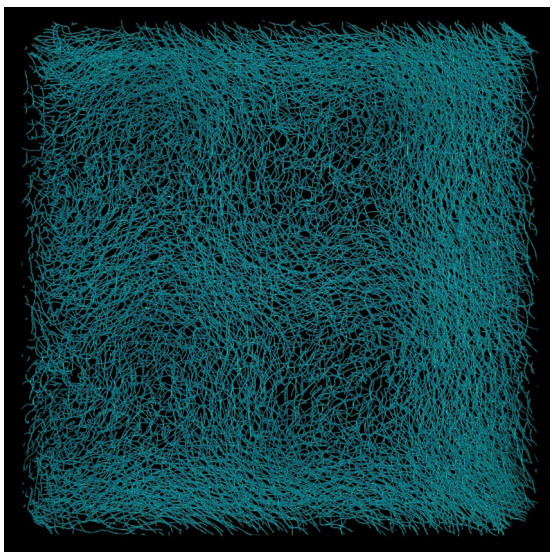

FIG. 5. Rendering of vortices at early times in a quantum ABC flow with helicity (spatial resolution of 2048^3 grid points). The regularized helicity is equal to 3, matching the value expected for the classical flow at large scales. Normalizing by the quanta, the helicity of this flow is $\approx 480\,000\Gamma^2$.

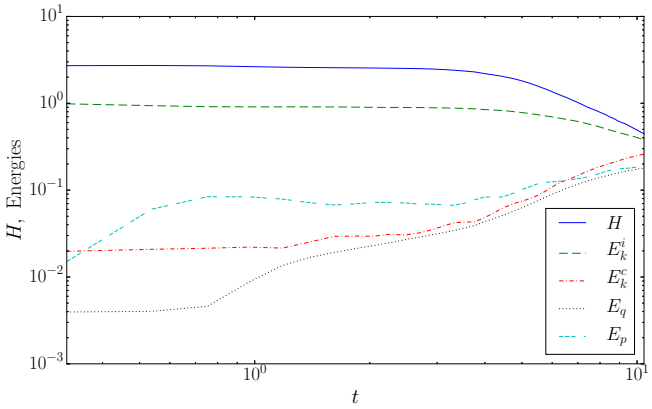

FIG. 6. Evolution of helicity and all energy components during the decay of a quantum turbulent flow with ABC initial conditions using 1024^3 grid points. Both helicity and the incompressible kinetic energy start to decay at around $t \approx 4$, in a correlated manner. The incompressible energy is redistributed into the other components, but the helicity is, in principle, dissipated.

the incompressible kinetic energy decays into compressible modes. Interestingly, the helicity is approximately conserved up to $t \approx 4$, but shortly before the incompressible kinetic energy starts to decay, so does the helicity. This behavior is reminiscent of the decay of energy and helicity in a freely decaying classical helical turbulent flow [43]. The decay of helicity at late times in Fig. 6 is probably due to the emission of phonons by Kelvin waves as observed in the trefoil knot (see Figs. 2 and 4), although further studies are needed to properly address this point.

VI. CONCLUSIONS

In a quantum flow the definition of helicity from classical hydrodynamics is ill defined, as it involves the integral of the product of two singular distributions, the velocity and the vorticity. However, the singular behavior of the velocity in the direction parallel to the vorticity is the result of an indeterminate $0/0$ form, and can be regularized to obtain an expression that matches the hydrodynamic definition of helicity at large scales while also satisfying topological definitions of the helicity based on the link, writhe, and twist of the quantum vortices.

We show that the regularized helicity can be used to study the evolution of simple knots and rings, yielding results compatible with topological methods to calculate the helicity. The regularized helicity can be also used successfully in more complex turbulent flows in which tracing hundreds of thousands of individual vortices may be unfeasible. Moreover, by studying reconnection and the subsequent time evolution of quantum knots we show that in cases in which a broad spectrum of Kelvin waves is excited, helicity can be slowly depleted as the Kelvin waves dissipate into phonos. In a fully developed helical quantum flow helicity remains constat at early times, and later decreases as the incompressible flow motions decay into compressible (sound) modes.

While the behavior of helicity in a quantum flow is reminiscent of that found in classical fluids, the results presented here also showcase a clear difference between the two cases: classical vortex tubes have an extra degree of freedom that quantum vortices do not, as a classical vortex tube has a finite width and as such can have any twist. Thus, a large-scale bundle of quantum vortices can have helicity and behave (as in the quantum ABC flow) in a way reminiscent of a classical fluid. However, as the bundle disentangles through reconnection and the helicity is transferred towards helical deformations of individual vortices, these deformations can decay into phonons. A detailed study of this transfer mechanism in quantum turbulence, and of the decay of helicity at late times, is left for future studies.

ACKNOWLEDGMENTS

The authors acknowledge financial support from Grant No. ECOS-Sud A13E01, and from computing hours in the CURIE supercomputer granted by Project TGCC-GENCI No. x20152a7493.

APPENDIX: FRENET-SERRET FRAME AND EQUATIONS

Given a 3D curve $\mathbf{r}(s)$, with $\mathbf{r} = (x,y,z)$ and $ds = \sqrt{dx^2 + dy^2 + dz^2}$, the standard Frenet-Serret tangent $\mathbf{T}$, normal $\mathbf{N}$, and binormal $\mathbf{B}$ vectors are defined as

$$\frac{d\mathbf{r}}{ds} = \mathbf{T}, \tag{A1}$$

$$\frac{d\mathbf{T}}{ds} \Big/ \left\| \frac{d\mathbf{T}}{ds} \right\| = \mathbf{N}, \tag{A2}$$

$$\mathbf{T} \times \mathbf{N} = \mathbf{B}. \tag{A3}$$

These obey the Frenet-Serret equations

$$\frac{d\mathbf{T}}{ds} = \kappa \mathbf{N}, \tag{A4}$$

$$\frac{d\mathbf{N}}{ds} = -\kappa \mathbf{T} + \tau \mathbf{B}, \tag{A5}$$

$$\frac{d\mathbf{B}}{ds} = -\tau \mathbf{N}, \tag{A6}$$

where κ is the curvature and τ is the torsion.

[1] A. Brandenburg and K. Subramanian, Phys. Rep. **417**, 1 (2005).

[2] E. N. Rasmussen and D. O. Blanchard, Weather Forecasting **13**, 1148 (1998).

[3] C. Rorai, D. Rosenberg, A. Pouquet, and P. D. Mininni, Phys. Rev. E **87**, 063007 (2013).

[4] R. Marino, P. D. Mininni, D. Rosenberg, and A. Pouquet, Phys. Rev. E **87**, 033016 (2013).

[5] H. K. Moffatt, J. Fluid Mech. **35**, 117 (1969).
[6] H. K. Moffatt and R. L. Ricca, Proc. R. Soc. London Ser. A **439**, 411 (1992).
[7] M. R. Dennis and J. H. Hannay, Proc. R. Soc. London Ser. A **461**, 3245 (2005).
[8] R. L. Ricca and M. A. Berger, Phys. Today **49**(12), 28 (1996).
[9] H. K. Moffatt, Proc. Natl. Acad. Sci. USA **111**, 3663 (2014).
[10] A. V. Vologodskii, N. J. Crisona, B. Laurie, P. Pieranski, V. Katritch, J. Dubochet, and A. Stasiak, J. Mol. Biol. **278**, 1 (1998).
[11] M. R. Dennis, R. P. King, B. Jack, K. O'Holleran, and M. J. Padgett, Nat. Phys. **6**, 118 (2010).
[12] H. Kedia, I. Bialynicki-Birula, D. Peralta-Salas, and W. T. M. Irvine, Phys. Rev. Lett. **111**, 150404 (2013).
[13] F. Hussain and K. Duraisamy, Phys. Fluids **23**, 021701 (2011).
[14] D. Kleckner and W. T. M. Irvine, Nat. Phys. **9**, 253 (2013).
[15] G. P. Bewley, M. S. Paoletti, K. R. Sreenivasan, and D. P. Lathrop, Proc. Natl. Acad. Sci. USA **105**, 13707 (2008).
[16] S. Zuccher, M. Caliari, A. W. Baggaley, and C. F. Barenghi, Phys. Fluids **24**, 125108 (2012).
[17] C. Rorai, K. R. Sreenivasan, and M. E. Fisher, Phys. Rev. B **88**, 134522 (2013).
[18] M. W. Scheeler, D. Kleckner, D. Proment, G. L. Kindlmann, and W. T. M. Irvine, Proc. Natl. Acad. Sci. USA **111**, 15350 (2014).
[19] C. E. Laing, R. L. Ricca, and D. W. L. Sumners, Sci. Rep. **5**, 9224 (2015).
[20] S. Zuccher and R. L. Ricca, Phys. Rev. E **92**, 061001 (2015).
[21] Y. Kimura and H. K. Moffatt, J. Fluid Mech. **751**, 329 (2014).
[22] D. S. Hall, M. W. Ray, K. Tiurev, E. Ruokokoski, A. H. Gheorghe, and M. Möttönen, Nat. Phys. **12**, 478 (2016).
[23] D. Kleckner, L. H. Kauffman, and W. T. M. Irvine, Nat. Phys. (unpublished).
[24] E. Fonda, D. P. Meichle, N. T. Ouellette, S. Hormoz, and D. P. Lathrop, Proc. Natl. Acad. Sci. USA **111**, 4707 (2014).
[25] W. Thomson, Philos. Mag. **10**, 155 (1880).
[26] E. Kozik and B. Svistunov, Phys. Rev. Lett. **92**, 035301 (2004).
[27] V. S. L'vov and S. Nazarenko, J. Exp. Theor. Phys. Lett. **91**, 428 (2010).
[28] P. Clark di Leoni, P. D. Mininni, and M. E. Brachet, Phys. Rev. A **92**, 063632 (2015).
[29] C. Nore, M. Abid, and M. E. Brachet, Phys. Fluids **9**, 2644 (1997).
[30] G. Krstulovic and M. Brachet, Phys. Rev. E **83**, 066311 (2011).
[31] M. J. Lighthill, *An Introduction to Fourier Analysis and Generalised Functions* (Cambridge University Press, Cambridge, 1958).
[32] K. Klenin and J. Langowski, Biopolymers **54**, 307 (2000).
[33] See Supplemental Material at http://link.aps.org/supplemental/10.1103/PhysRevA.94.043605 for videos showing the evolution of the trefoil and the two rings knots.
[34] D. O. Gómez, P. D. Mininni, and P. Dmitruk, Adv. Space Res. **35**, 899 (2005).
[35] D. O. Gómez, P. D. Mininni, and P. Dmitruk, Phys. Scr. **2005**, 123 (2005).
[36] P. Mininni, D. Rosenberg, R. Reddy, and A. Pouquet, Parallel Comput. **37**, 316 (2011).
[37] M. V. Berry and M. R. Dennis, Eur. J. Phys. **33**, 723 (2012).
[38] L. Boué, D. Khomenko, V. S. L'vov, and I. Procaccia, Phys. Rev. Lett. **111**, 145302 (2013).
[39] P. C. di Leoni, P. Cobelli, and P. Mininni, Eur. Phys. J. E **38**, 1 (2015).
[40] W. F. Vinen, M. Tsubota, and A. Mitani, Phys. Rev. Lett. **91**, 135301 (2003).
[41] S. K. Nemirovskii and A. J. Baltsevich, in *Quantized Vortex Dynamics and Superfluid Turbulence*, Lecture Notes in Physics No. 571, edited by C. F. Barenghi, R. J. Donnelly, and W. F. Vinen (Springer, Berlin, 2001), pp. 219–225.
[42] S. K. Nemirovskii, Phys. Rep. Quantum Turbulence **524**, 85 (2013).
[43] T. Teitelbaum and P. D. Mininni, Phys. Fluids **23**, 065105 (2011).